DOI: 10.1002/ejic.200700490

Synthesis, Characterization, and Photoluminescence Properties of In_2O_3 Nanocrystals Encapsulated by Carbon Vesicles and Neat In_2O_3 Nanocrystals Generated by the RAPET Technique

Pani P. George[a] and Aharon Gedanken*[a]

Keywords: Decomposition / Indium / Luminescence / Nanocrystals / Vesicles

We report the synthesis of micron-sized vesicles of carbon encapsulating In_2O_3 nanocrystals, as well as neat In_2O_3 nanocrystals. The thermal decomposition of $In(acetate)_3$ was carried out at 800 °C in air. This reaction was carried out under the autogenic pressure of indium acetate. The synthesized products were systematically characterized by X-ray powder diffraction, scanning electron microscopy, and transmission electron microscopy. Carbon microvesicles, with an average diameter of 5 μm, encapsulated several nanometric-sized In_2O_3 nanocrystals, as evidenced by high resolution transmission electron microscopy. The UV/Vis absorption of In_2O_3 nanocrystals was studied to estimate the bandgap energies.

Introduction

Semiconductor nanostructures have been attracting increasing attention because of their exceptional properties, which differ from those of their bulk counterparts, and because of their potential application in optoelectronic devices. Research on nanostructures provides the potential for a variety of chemical, electronic, catalytic, electrochemical, and photonic applications.[1–3] The electrical, optical, and magnetic properties of nanostructures vary with factors such as size, shape, and crystallinity. In particular, nanophase composite structures, which consist of nanoparticles in a matrix material, can have properties significantly different from those of the matrix.

Indium oxide (In_2O_3) has been investigated extensively for its semiconducting properties. It is a very important wide-bandgap (direct-bandgap around 3.6 eV), n-type transparent semiconductor, and it has been widely used in microelectronic areas, including window heaters, solar cells, liquid–crystal displays, and ultrasensitive gas sensors for the detection of O_3, CO_2, H_2, NO_2, and Cl_2. To date, various morphologies of In_2O_3 have been synthesized, for example, nanofibers,[4] metal-filled nanotubes,[5] ordered nanowire arrays,[6–7] nanoparticles dispersed within pores of mesoporous silica,[8–9] and size-controlled In_2O_3 nanoparticles.[10–11] In addition, there are one-step reactions for the synthesis of In_2O_3 nanocrystals.[25–26] To the best of our knowledge, there is no report on the formation of carbon vesicles encapsulating In_2O_3 nanocrystals or on neat In_2O_3 nanocrystals prepared under autogenic pressure at elevated temperature. In this article, we describe a simple one-step, solvent-free, and efficient method for the synthesis of highly crystalline In_2O_3 nanocrystals by employing the RAPET (reactions under autogenic pressure at elevated temperatures) method. The advantage of this method over other techniques is that the as-prepared samples are already nanocrystalline in nature.

[a] Department of Chemistry and Kanbar Laboratory for Nanomaterials, Bar-Ilan University Center for Advanced Materials & Nanotechnology,
Bar-Ilan University, Ramat-Gan, Israel
Fax: +972-3-535-1250
E-mail: gedanken@mail.biu.ac.il

Characterization

The XRD patterns of samples A and B were recorded with a Bruker D8 diffractometer with Cu-K_α radiation. C and H analyses was carried out with an Eager 200 CE instrument and an EA 1110 Elemental Analyzer. The morphologies of the sample and also of the annealed product were studied by scanning electron microscopy (SEM), coupled with energy-dispersive X-ray (EDX) analysis. EDX analysis was carried out with a JEOL micrograph (JEOL 2010 operated at 200 kV). Transmission electron microscopy (TEM) studies were carried out with a JEOL 2000 electron microscope. High-resolution TEM (HRTEM) images were obtained with a JEOL 2010 at an accelerating voltage of 200 kV. Samples for the TEM and HRTEM measurements were obtained by placing a drop of the suspension from the sonicated reaction product in ethanol onto a carbon-coated copper grid, followed by drying in air to remove the solvent. Optical absorption spectra were measured with a Shimadzu UV-2100 spectrophotometer at room temperature. Photoluminescence measurements were

performed with a Perkin–Elmer Luminescence spectrometer L550B at room temperature.

Results and Discussion

Powder X-ray Diffraction (PXRD), Elemental (C and H), SEM, HRSEM, and EDX Analysis

The XRD patterns of thermally decomposed In(acetate)$_3$ at 800 °C in a closed Letlok cell in air are presented in Figure 1a, and a representative XRD pattern for our as-synthesized carbon-encapsulated indium oxide nanocrystals is also displayed. All the main peaks can be indexed undisputedly to In_2O_3 [powder diffraction file (PDF) no. 03-065-3170]. The degree of carbon graphitization was deduced from the PXRD results. The absence of graphite peaks indicates the possibility that carbon is present only as amorphous carbon. The diffraction peaks at 2θ = 21.4, 30.5, 35.3, 37.6, 45.5, 50.9, 50.9, 55.8, and 60.5° are assigned to (211), (222), (400), (411), (134), (440), and (611) planes of In_2O_3, respectively. From the (222) diffraction peak, the average interlayer spacing was calculated to be 3.15 Å. The average crystallite size for In_2O_3@C and In_2O_3 was calculated to be ca. (20 ± 2) nm by using the Debye–Scherrer equation.

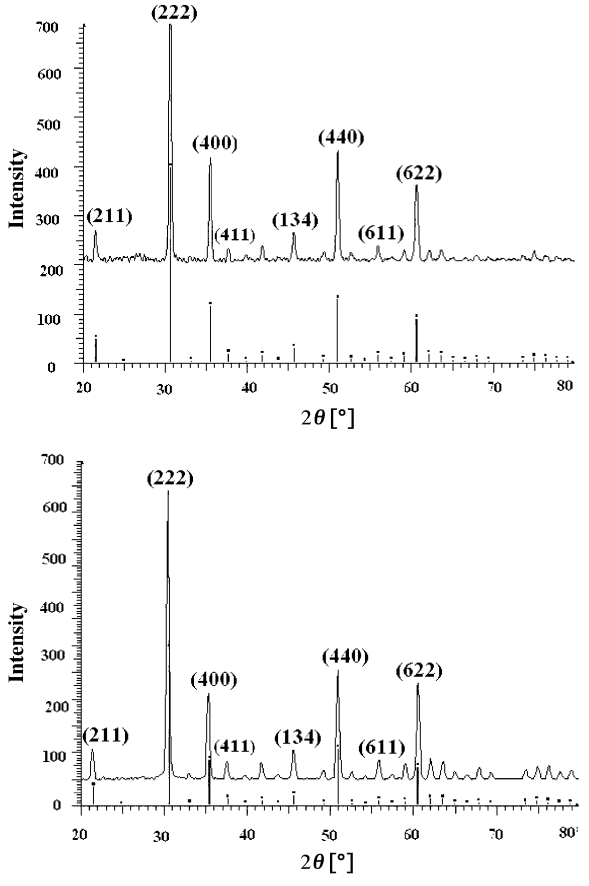

Figure 1.PXRD pattern of: The thermally decomposed In(acetate)$_3$ at 800 °C in air (top). The thermally decomposed In(acetate)$_3$ at 800 °C in air and further annealed at 500 °C in air for 3 h (bottom).

By considering the presence of a uniform layer of carbon coated onto the surface of In_2O_3, which will be shown later, the formed product was termed an "indium oxide–carbon" (IOC) composite. To eliminate the carbon, the IOC core–shell was annealed at 500 °C in air. The elemental (C, H, N, S) analysis detected 0% carbon and 0% hydrogen in the product after the annealing process. In Figure 1b, a representative PXRD pattern of neat indium oxide nanocrystals is displayed. The diffraction peaks, peak intensities, and cell parameters are in agreement with the diffraction peaks of the crystalline body-centered cubic phase of In_2O_3 (PDF No. 03-065-3170). The peaks of body-centered cubic In_2O_3 are narrower than those of the In_2O_3@C sample, which indicates crystallite growth that is either due to the sintering of neighboring particles or to the release of microstrains during the annealing process.

The calculated elemental percentages of C, H, O, and In in the In(acetate)$_3$ precursor are 19.7, 3, 35.0, and 42.0%, respectively. We could determine the carbon and hydrogen content in the In_2O_3@C sample with an elemental (C, H, N, and S) analyzer. The measured amount of carbon in the In_2O_3@C sample was 10.43%, whereas the amount of hydrogen was reduced to 0.07%. It is clear that the amount of carbon and hydrogen in the In_2O_3@C sample is reduced relative to the precursor, because gases such as CO_2, C_xH_y (hydrocarbons), and/or H_2 are formed during the decomposition of the precursor. These gases are liberated as a result of overpressure and upon the opening of the closed Letlok cell.[12–14]

Structure and Morphology

Carbon vesicles encapsulating In_2O_3 nanocrystals were synthesized by the thermal dissociation of In(acetate)$_3$ at an elevated temperature of 800 °C under autogenic pressure. The morphologies of the In_2O_3@C core–shell nanoparticles and the In_2O_3 nanocrystals obtained after annealing at 500 °C in air were primarily investigated by SEM measurements. The SEM image of the IOC sample at low- and high magnifications are shown in Figure 2. From the SEM observations, it can be seen that the IOC product is composed of carbon vesicles; many of them have a cauliflower structure, and some of them are agglomerated. In addition, there are particles of irregular and nonuniform morphologies. The surface of the carbon material is rough. Sun et al. demonstrated that the carbon fiber surface became rough after plasma treatment.[15] The average diameter of each carbon micron vesicle was 6 μm. The thickness of folded carbon ranged from 1.6–3.2 μm. Elemental analysis measurements of the IOC core–shell revealed the presence of C in the sample. Figure 2b demonstrates the SEM images of neat In_2O_3 obtained after annealing the In_2O_3@C sample at 500 °C in air. As stated above, the carbon coverage completely disappeared after the annealing treatment. A bundle of nanocrystals appears in the SEM images (Figure 2b). This nanocrystal bundle assembly might be due to the sintering of the crystals, which occurs upon annealing at 500 °C in air for 3 h. The thickness of the nanoparticles composed in the bundle is in the range of 85–120 nm and the length is in the

range of 85–200 nm. The average size of the nanocrystal bundle is 350 nm. EDX measurements of In_2O_3@C micron vesicles and neat In_2O_3 nanocrystals indicate the presence of only indium and oxygen, and no other impurities are observed. The composition of the In_2O_3@C and neat In_2O_3, obtained from EDX analysis gives an In/O atomic ratio ≈ 1.5:1 in agreement with In_2O_3.

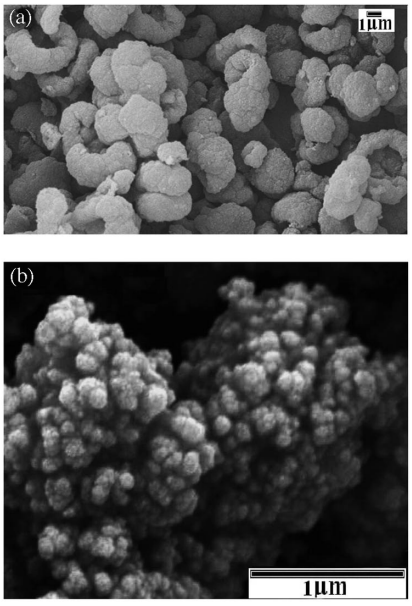

Figure 2.(a) SEM image of the IOC structure; (b) SEM image of neat In_2O_3 nanocrystals obtained after annealing the In_2O_3@C micron vesicles at 500 °C in air for 3 h.

TEM and HRTEM Measurements

The structure of the In_2O_3@C product was further studied by TEM and HRTEM measurements. Figure 3 demonstrates the portion of the micron-sized carbon vesicle obtained by the thermal decomposition of In(acetate)$_3$ at 800 °C. The In_2O_3@C vesicle has an average diameter of 0.7 μm. The TEM measurements indicate that the carbon vesicle was composed of several hollow carbon spheres with an average wall thickness of less than 9 nm. Only a few hollow carbon spheres encapsulate In_2O_3 nanoparticles, and the remaining hollow carbon spheres remain empty. The diameters of the hollow carbon spheres and In_2O_3 nanoparticles encapsulated within the carbon spheres are in the range of 50–140 nm and 35–140 nm, respectively. As the diameters of the hollow spaces (ca. 50 nm) were about the same as the diameter of the In_2O_3 nanoparticles (ca. 50 nm), we consider that the In_2O_3 nanoparticles acted as a mold to form the hollow structure of the carbon. Similar hollow carbon spheres encapsulating Pt nanoparticles were earlier demonstrated by Ikeda, et al.[17]

The TEM image reveals that most of the In_2O_3 nanoparticles encapsulated within the hollow carbon spheres are spherically shaped, although some are irregular plate shaped. Therefore, it should be noted that In_2O_3 nanoparticles synthesized by the RAPET technique exhibit an irregular plate shape, as well as a spherical morphology. The spherical shape of our nanoparticles differs from the wire-shaped In_2O_3 nanoparticles obtained by Dai et al.[19] The synthetic strategy of Dai involves the silicon substrate, pure indium balls, and H_2O, and the reaction was conducted under an argon flow at 850 °C. The current RAPET synthetic approach involves a simpler precursor, In(acetate)$_3$, and it does not require solvents, any substrate, or an argon atmosphere for the formation of spherically shaped In_2O_3 nanoparticles. The nanowires prepared by the synthetic strategy of Dai have diameters ranging from 20 to 50 nm and are smaller than those of the spherical In_2O_3 nanoparticles (40–90 nm) produced under Letlok reaction conditions.

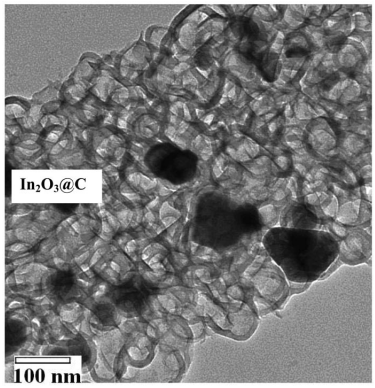

Figure 3.TEM image of In_2O_3@C micron vesicles.

To obtain the detailed structure and composition of individual carbon micron vesicles, an HRTEM image was taken, and SAED and selected area energy dispersive X-ray spectroscopy (SAEDS) measurements were carried out. Figure 4a represents the HRTEM image of carbon micron vesicle encapsulating crystalline nanoparticles of In_2O_3, and Figure 4b portrays the corresponding ED pattern. In addition, we measured the selected area EDS of the carbon (light-colored region) encapsulating the In_2O_3 nanoparticles. The SAEDS spectrum of the light-colored region showed mainly carbon. The ED pattern (Figure 4b) focused on the black particles, which provides evidence for the crystalline nature of In_2O_3 (the detected planes are shown). We

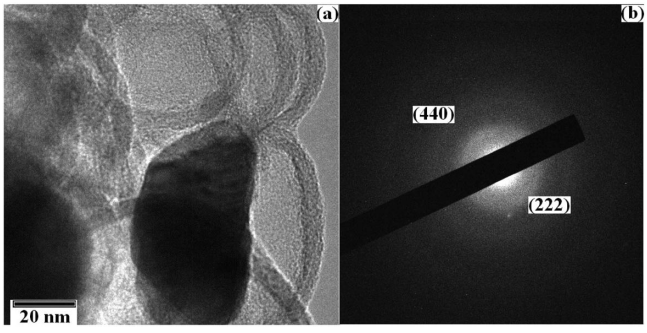

Figure 4.(a) HRTEM photograph of carbon-encapsulated nanocrystals of In_2O_3 and the corresponding microdiffraction; (b) the picture was measured with a HRTEM instrument.

did not observe any graphite peaks in the PXRD. This confirms that the carbon coated onto the In_2O_3 nanocrystals is amorphous in nature.

Neat Indium Oxide Nanocrystalline Morphologies

Figure 5 depicts the TEM image of the morphology of the neat In_2O_3 nanocrystals, which is the major structure observed in the picture. They are obtained after annealing the In_2O_3@C micron vesicles at 500 °C. The neat In_2O_3 nanocrystals have diameters between 35 and 120 nm and lengths between 50 and 140 nm, which is consistent with the values of In_2O_3 nanoparticles encapsulated in the carbon vesicles of the IOC sample. From the HRTEM image (Figure 4a), the carbon in In_2O_3@C acts as a cover and envelops the nanocrystals of In_2O_3 with variable shapes. Once the carbon cover is removed, the basic shape of the indium oxide and the nanocrystals is exposed. Recently, Russel, et al. demonstrated the synthesis of similar In_2O_3 nanocrystals.[11]

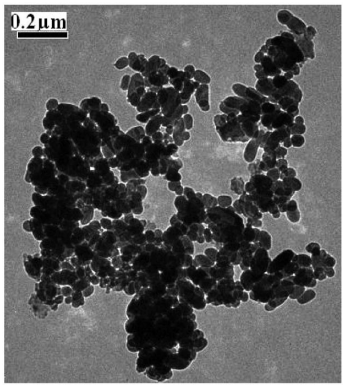

Figure 5.TEM images of neat In_2O_3 nanocrystals.

The HRTEM, SAED, and selected area energy dispersive X-ray spectroscopy (SAEDS), measurements were carried out on In_2O_3 nanocrystals obtained after annealing the In_2O_3@C sample in air at 500 °C. Figure 6a and b represent the HRTEM images of In_2O_3 nanocrystals with an average length of 60 nm and an average thickness of 48 nm. Figure 6b is the high-magnification image of one of the In_2O_3 nanoparticles. An interlayer spacing of 0.298 nm is measured for the (222) plane of the In_2O_3 nanoparticle. The measured distance between these (222) lattice planes is very close to the distance between the planes reported in the literature (0.292 nm) for the body-centered cubic lattice of indium oxide (PDF: 03-065-3170). The ED pattern (Figure 6c) provides evidence for the crystalline nature of In_2O_3 (the detected planes are shown). The presence of a few disordered spots in the ED pattern is attributed to the interference from the diffractions of neighboring In_2O_3 nanocrystals. To identify the dark nanosized particles (HRTEM Figure 6b) we measured a selected area EDS analysis. The measurements from the spectrum (Figure 6d) demonstrate the existence of 83.2 wt.-% of In and 16.8 wt.-% of O, which is very close to the theoretical value of In_2O_3 (In 82.7 wt.-% and O 17.2 wt.-%). No other impurities were found in the EDAX measurements.

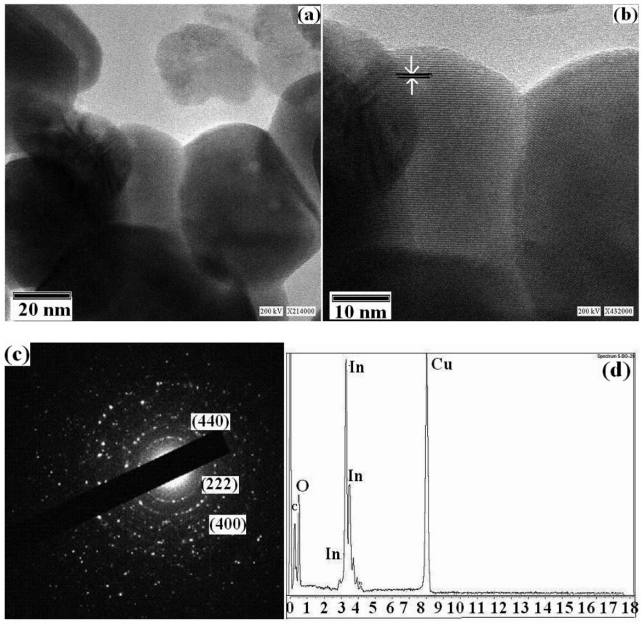

Figure 6.(a) HRTEM image of In_2O_3 nanocrystals; (b) high-magnification image of In_2O_3 nanocrystals; (c) corresponding electron diffraction; (d) selected area EDS analysis of neat nanosized In_2O_3 crystals.

Optical Properties of In_2O_3 Nanocrystals

As a promising model for transparent conducting oxide materials, In_2O_3 plays an important role in manufacturing optoelectronic devices. Many investigations have been carried out on the optical properties of the In_2O_3 nanoparticles. UV/Vis spectra and photoluminescence (PL) spectra were recorded with ethanol used as the reference. An estimate of the optical bandgap is obtained by using the following equation for a semiconductor:[17]

$\alpha(\nu) = A(\hbar\nu/2 - E_g)^{m/2}$,

where $\hbar = h/\pi$, $\hbar\nu$ is the photon energy, α is the absorption coefficient, and m is dependent on the nature of the transition. For a direct transition, m is equal to 1 or 3, whereas for an indirect-allowed transition, m is equal to 4 or 6. Because A is proportional to $F(R)$, the Kubelka–Munk function $F(R) = (1 - R)^2/2/R$, the energy intercept of a plot of $[F(R)*h\nu]^2$ and $[F(R)*h\nu]^{1/2}$ vs. $h\nu$ yields the $E_{g,dir}$ for a direct-allowed transition and the $E_{g,ind}$ for an indirect-allowed transition, respectively, when the linear regions are extrapolated to the zero ordinate.[17]

The PL spectrum of the In_2O_3 nanocrystals was measured with an F-850 fluorescence spectrophotometer (Hitachi) by using an excitation wavelength of 325 nm at room temperature. It is known that bulk In_2O_3 cannot emit light at room temperature.[18–20] Earlier reports indicated that In_2O_3 nanoparticles have PL peaks at 480 and 520 nm. In_2O_3 nanofibers exhibit broad PL emission peaks centered at 470 nm,[21] and In_2O_3 nanowires synthesized by the EDO

method display strong PL emission peaks centered at 425, 429, 442, and 460 nm.[4,22] Cao and coworkers observed a strong emission for In_2O_3 nanowires, even in the ultraviolet region, which is attributed to near band-edge emission instead of the defect-induced emission.[6,22] The IOC sample does not show any PL peaks (Figure 7c) under UV light. We anticipate that the carbon encapsulating the In_2O_3 nanoparticles inhibits the In_2O_3 nanocrystals from absorbing UV radiation. Indeed, the comparison of the absorption spectra of In_2O_3@C and neat In_2O_3 substantiate this explanation. Figure 7a and Figure 7b present the UV/Vis absorption spectrum of two colloidal solutions of In_2O_3@C nanocrystals and neat In_2O_3 nanocrystals dispersed in ethanol, respectively. Although the absorption of the neat In_2O_3 nanocrystals starts at 800 nm and increases through the visible region, it is considerably smaller than that of the In_2O_3@C nanocrystals. The latter absorbs the exciting light in the visible region and photons cannot excite the In_2O_3 in the core. In contrast, the opposite is true for neat In_2O_3 where minimal absorption does not stop the excitation of the core and PL is therefore detected at the expected wavelengths.

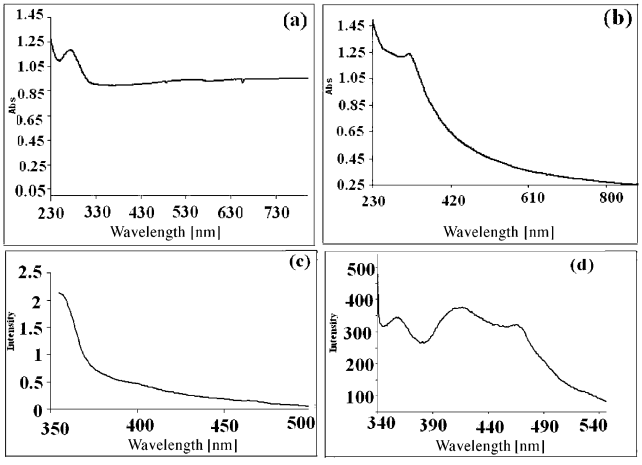

Figure 7.(a) Room temperature UV/Vis absorption spectrum of In_2O_3@C nanocrystals; (b) room temperature UV/Vis absorption spectrum of In_2O_3 nanocrystals; (c) photoluminscence spectrum of In_2O_3@C nanocrystals at room temperature excited at 275 nm; (d) photoluminscence spectrum of In_2O_3 nanocrystals at room temperature excited at 325 nm. The measurements were made in the absorption mode.

Figure 7d shows a broad PL emission spectrum recorded for the In_2O_3 nanocrystals with a thickness of 56–230 nm excited by 325 nm photons. The emission is mainly located in the blue-green region with fluorescence peaks centered at 360, 410, and 460 nm. The different emission peaks are related to the different energy levels produced by the oxygen vacancies caused during the annealing process.

Discussion

The basic requirement that must be fulfilled for a successful RAPET reaction is that a thermodynamic driving force must exist for the reaction to proceed with no sustained external energy. In the current study, the production of In, O_2, C, and H_2 in the gaseous phase provides the enthalpic drive for the transformation of In(acetate)$_3$ into In_2O_3 nanocrystals.[15–17] Under RAPET conditions, In(acetate)$_3$ dissociates into carbon, hydrogen, oxygen, and indium atoms. As in MPI (multiphoton ionization) experiments on the metal carbonyls, where metal atoms (W, Cr, etc.) are detected in the gas phase,[24] all the dissociated products of In(acetate)$_3$ will float in the gas phase. As the reaction proceeds, the indium and oxygen atoms react in the gas phase to eventually form In_2O_3 nanocrystals. The occurrence of oxide nanoparticles by the RAPET reaction of metal alkoxides was earlier demonstrated by us in a series of papers.[12–14,23]

The carbon vesicles encapsulating the In_2O_3 nanocrystals are the result of the disproportionation of aliphatic and aromatic hydrocarbons. The carbon layer encapsulating the In_2O_3 nanocrystals resembles a similar carbon obtained in many RAPET experiments on metal alkoxides, explained by their faster kinetics.[12–14,24]

Conclusions

In this article, micron-sized carbon vesicles encapsulating In_2O_3 nanocrystals and neat In_2O_3 nanocrystals were successfully generated by the RAPET method. The RAPET technique is an effective method for preparing In_2O_3 nanocrystals. The method presented herein is a novel, simple, and efficient reaction for the direct preparation of core–shell nanoparticles by a single step process, i.e., annealing the In_2O_3@C micron vesicles at 500 °C in air to produce pure In_2O_3 nanocrystals. The formation mechanism for the In_2O_3 nanostructures is based on an aggregation process of primary nanoparticles. The In_2O_3 nanocrystals show a blue emission due to the oxygen vacancies.

Experimental

The synthesis of In_2O_3@C micron vesicles is carried out by the thermal dissociation of indium triacetate, In(acetate)$_3$, which was purchased from Aldrich and used as received. The 3-mL closed-vessel cell was assembled from stainless steel Letlok parts (manufactured by the HAM-LET Co., Israel). A one-half inch union part was plugged from both sides by standard caps, as described previously.[13] For the synthesis, In(acetate)$_3$ (1.0 g) was introduced into the cell at room temperature in air. The filled cell was closed tightly by the other plug and then placed inside an iron pipe in the middle of the furnace. The temperature was raised at a heating rate of 10 °C min^{-1}, and the closed-vessel cell was heated at 800 °C for 3 h. The reaction took place under the autogenic pressure of the precursor. At the end of the reaction, the Letlok was gradually cooled (5 h) to room temperature, and after opening, a black powder (0.69 g) was obtained. The total yield of the product material was 69% of the total weight of the materials introduced into the cell. [The yield is defined as the final weight of the product relative to the weight of In(acetate)$_3$, the starting material]. The synthesis of nanomaterials by the RAPET method required the use of simple equipment and a short reaction time to create carbon vesicles encapsulating the In_2O_3 nanocrystals (SAMPLE A). The prepared

In_2O_3@C nanocrystals were further annealed at 500 °C in air for 3 h. The annealing removes the carbon layer and leads to the formation of green-colored In_2O_3 nanocrystals (SAMPLE B).

Acknowledgments

We thank the Bar-Ilan Research authority for providing the facilities to carry out this work. Technical support from Dr. Yuri Koltypin is gratefully acknowledged. This research was partially supported by a grant from The Ministry of Science, Culture, and Sport through the Strategic Fundamental Program

[1] M. H. Huang, Y. Wu, H. Fieck, N. Tran, E. Weber, P. Yang, *Adv. Mater.* **2001**, *13*, 113.
[2] Z. L. Wang, R. P. Gao, J. D. Stout, *Adv. Mater.* **2000**, *12*, 1938.
[3] P. Yang, C. M. Lieber, *Science* **1996**, *273*, 1836.
[4] C. H. Liang, G. W. Meng, Y. Philipp, L. D. Zhang, *Adv. Mater.* **2001**, *13*, 1330.
[5] Y. Li, Y. Bando, D. Golberg, *Adv. Mater.* **2003**, *15*, 581.
[6] M. J. Zheng, L. D. Zhang, G. H. Li, X. Y. Zhang, X. F. Wang, *Appl. Phys. Lett.* **2001**, *79*, 839.
[7] H. F. Yang, Q. H. Shi, B. Z. Tian, Q. Y. Lu, F. Gao, S. H. Xie, J. Fan, Z. Yu, B. Tu, D. Y. Zhano, *J. Am. Chem. Soc.* **2003**, *125*, 4724.
[8] H. J. Zhou, W. P. Cai, L. D. Zhang, *Appl. Phys. Lett.* **1999**, *75*, 495.
[9] H. J. Zhou, W. P. Cai, L. D. Zhang, *Mater. Res. Bull.* **1999**, *34*, 845.
[10] W. S. Seo, H. H. Jo, K. Lee, J. T. Park, *Adv. Mater.* **2003**, *15*, 795.
[11] R. Garkova, G. Volksch, C. Russel, *J. Non-Cryst. Solids* **2006**, *352*, 5265.
[12] S. V. Pol, V. G. Pol, V. G. Kessler, G. A. Seisenbaeva, M. Sung, S. Asai, A. Gedanken, *J. Phys. Chem. B* **2004**, *108*, 6322.
[13] S. V. Pol, V. G. Pol, A. Gedanken, *Chem. Eur. J.* **2004**, *10*, 4467.
[14] V. G. Pol, S. V. Pol, A. Gedanken, Y. Goffer, *J. Mater. Chem.* **2004**, *14*, 966.
[15] Q. Zhu, J. Sun, C. He, J. Zhang, Q. Wang, J. Macro, *Pure Appl. Chem. Sci. A* **2006**, *43*, 1853.
[16] S. V. Pol, V. G. Pol, V. G. Kessler, A. Gedanken, *New J. Chem.* **2006**, *30*, 370.
[17] V. Luca, S. Djajanti, R. F. Howe, *J. Phys. Chem. B* **1998**, *102*, 10650.
[18] K. Soulantica, L. Erades, M. Sauvan, F. Senocq, A. Maisonnat, B. Chaudret, *Adv. Funct. Mater.* **2003**, *13*, 553.
[19] L. Dai, X. L. Chen, J. K. Jian, M. He, T. Zhou, B. Q. Hu, *Appl. Phys. A* **2002**, *75*, 687.
[20] Y. H. Ng, S. Ikeda, T. Harada, S. Higashida, T. Sakat, H. Mori, M. Matsumura, *Adv. Mater.* **2007**, *19*, 597.
[21] H. B. Jia, Y. Zhang, X. H. Chen, J. Shu, X. H. Luo, Z. S. Zhang, D. P. Yu, *Appl. Phys. Lett.* **2003**, *82*, 4146.
[22] X. S. Peng, G. W. Meng, J. Zhang, X. F. Wang, Y. W. Wang, C. Z. Wang, L. D. Zhang, *J. Mater. Chem.* **2002**, *12*, 1602.
[23] P. P. George, V. G. Pol, A. Gedanken, *Nanoscale Res. Lett.* **2007**, *2*, 17.
[24] G. J. Fisanick, A. Gedanken, T. S. Eichelberger, N. A. Kuebler, M. B. Robin, *J. Chem. Phys.* **1981**, *75*, 5215.
[25] N. Pinna, G. Neri, M. Antonietti, M. Niederberger, *Angew. Chem. Int. Ed.* **2004**, *43*, 4345.
[26] M. Niederberger, G. Garnweitner, J. Buha, J. Polleux, J. Ba, N. Pinna, *J. Sol-Gel Sci. Technol.* **2006**, *40*, 259.

Received: May 7, 2007
Published Online: August 9, 2007

